EVS27
Barcelona, Spain, November 17 - 20, 2013

From Accelerated Aging Tests to a Lifetime Prediction Model: Analyzing Lithium-Ion Batteries

Johannes Schmalstieg[1,3], Stefan Käbitz[1,3], Madeleine Ecker[1,3], and Dirk Uwe Sauer[1,2,3]

[1] *Electrochemical Energy Conversion and Storage Systems Group, Institute for Power Electronics and Electrical Drives (ISEA), RWTH Aachen University, Jaegerstrasse 17/19, 52066 Aachen, Germany, jsc@isea.rwth-aachen.de*
[2] *Institute for Power Generation and Storage Systems (PGS), E.ON ERC, RWTH Aachen University, Germany*
[3] *Jülich Aachen Research Alliance, JARA-Energy, Germany*

Abstract

As lithium-ion batteries play an important role for the electrification of mobility due to their high power and energy density, battery lifetime prediction is a fundamental aspect for successful market introduction. This work shows the development of a lifetime prediction model based on accelerated aging tests. To investigate the impact of different voltages and temperatures on capacity loss and resistance increase, calendar life tests were performed. Additionally, several cycle aging tests were performed using different cycle depths and mean SOC. Both the calendar and the cycle test data were analyzed to find mathematical equations that describe the aging dependence on the varied parameters. Using these functions an aging model coupled to an impedance-based electrical-thermal model was built. The lifetime prognosis model allows analyzing and optimizing different drive cycles and battery management strategies. The cells modeled in this work were thoroughly tested taking into account a wide range of influence factors. As validation tests on realistic driving profiles show, a robust foundation for simulation results is granted. Together with the option of using temperature profiles changing over the seasons, this tool is able to simulate battery aging in various applications.

Keywords: lithium battery, battery model, battery calendar life, cycle life, simulation

1 Introduction

Lithium-ion batteries are a key technology for current and future energy storage, whether they are used for mobile or stationary application. As the batteries' portion of cost is quite high for many applications, battery lifetime is a critical point for profitability. However, performing real life aging tests for every single application is an expensive and time consuming process which cannot be done in every case. Aging models based on accelerated aging tests can overcome this challenge as they have to be done only once per cell type. Using mathematical functions to

reproduce the factors influencing aging, such as temperature or storage voltage, allows an extrapolation from a fixed set of accelerated tests to a wide range of applications.

To give an aging prediction a lot of different aging factors need to be accounted for, including temperature, storage voltage, charge throughput and cycle depth [1, 2]. Some studies have already published simulations dealing with a few of these factors, either calendar life [3, 4, 5, 6] or cycle life [7]. Completely parameterized models including all of these factors and considering both calendar and cycle life are still missing.

This paper shows an accelerated aging test set including more than sixty cells of a high-energy 18650 system with NMC cathode material. Both capacity loss as well as resistance increase are addressed. Calendar and cycle aging are considered separately. A holistic aging model is presented with an impedance based electric-thermal model. Finally the comparison between simulation results and verification measurements at nine different conditions will be shown.

2 Experimental

The tested battery was the Sanyo UR18650E, an 18650 round cell which is manufacturer rated with 2.05 Ah minimum and 2.15 Ah typically. The cathode active material is Li(NiMnCo)O_2 (NMC) and the anode consists of graphite. It is a high energy cell with a maximum discharge rate of 3C and 165 Wh/kg energy density. Voltage limits are 2.5 V for discharging and 4.2 V for charging with a proposed end of discharge voltage of 3.0 V and end of charge voltage of 4.1 V. An OCV curve of the cell is shown in figure 1.

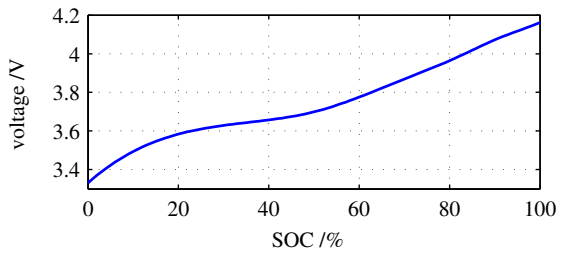

Figure 1: OCV curve for the cell used.

2.1 Calendar aging matrix

A list of all tested calendar aging test conditions can be found in figure 2. As the temperature dependency with an Arrhenius equation is already described by some authors ([1, 8]), only three different temperatures are tested to verify this dependency. More attention was given to the voltage dependency, which is highly resolved with 10 different conditions. Each combination of temperature and voltage in the calendar aging test consists of three cells to get some statistics. All cells were held at a constant voltage (float conditions) during the tests. Every seven weeks a measurement of the cells capacity and inner resistance was performed.

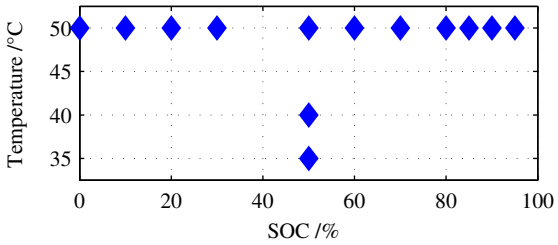

Figure 2: Test matrix of calendar aging tests.

2.2 Cycle aging matrix

The main focus of the cycle aging tests was the cycle depth and the mean SOC. A diagram with all cycle aging test conditions can be found in figure 3. All cycling tests were done at a current rate of 1C and a cell temperature of 35 °C. Temperature was logged using a sensor mounted on the surface of the cell. The mean SOC was set by a constant voltage charge using the OCV curve of the cell. Cycling was done Ah based around this point, with a reset of the mean SOC every 100 cycles. If a test had 0 or 100 % SOC as limit, these points were used to set the cycle range. Checkups measuring the capacity and the inner resistance of the cell were made every 3 weeks.

2.3 Checkups

All capacity and resistance measurements were done at 35 °C. The capacity measurement starts with a standard charge which is a 1C charge up to 4.2 V followed by a CV charge until current was below C/50. After that the capacity

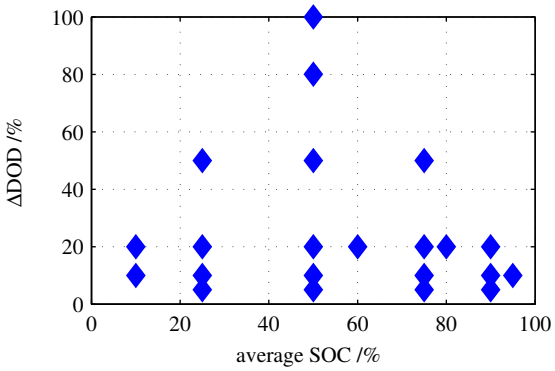

Figure 3: Test matrix of cycle life tests performed on a 2.05 Ah cell.

was measured during the 1C discharge down to 2.5 V. The inner resistance was measured at SOC steps of 10 %, starting from 90 % SOC down to 10 % SOC. Every step was reached Ah based by discharging 1/10 of capacity starting from a completely charged battery in the first step. At each step a pulse power characterization profile (PPCP) is applied to the battery. The PPCP consists of an 18 s 2C discharge followed by a 40 s rest period. After that a 10 s 1C charge is applied, again followed by a 40 s rest period. A voltage response to this PPCP is shown in figure 4. From this profile various inner resistances are calculated, a 2, 10 and 17 s resistance for the discharge and a 2 and 10 s resistance for the charge. For the aging calculation the 10 s discharge resistance at 50 % SOC is used. This resistance is calculated as the difference between the voltage before the discharge pulse and 10 s after the beginning of the discharge pulse divided by the current. All other resistances are calculated in a similar way.

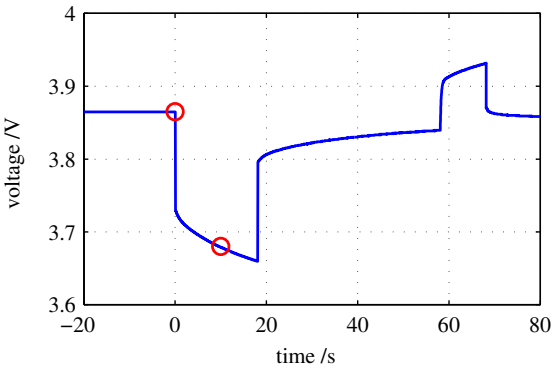

Figure 4: Voltage reaction of a new cell to a PPCP. The two voltages used for calculating the 10 s discharge resistance are marked red.

3 Calendar aging

In the calendar aging tests, cells were stored at different temperatures and voltages. Each test condition was performed with 3 cells to demonstrate the reproducibility of the experiment. The results show a very similar aging for cells tested under the same conditions, the measured capacities show an especially great uniformity.
Only the tests at 100 % had a difference of more than 4 percentage points between the best and worst cell. As these cells also had a very strong aging, they are excluded from further analysis. With a storage voltage of 4.162 V they were above the recommended end of charge voltage. This might lead to additional aging effect which cannot be scaled down to lower voltages.

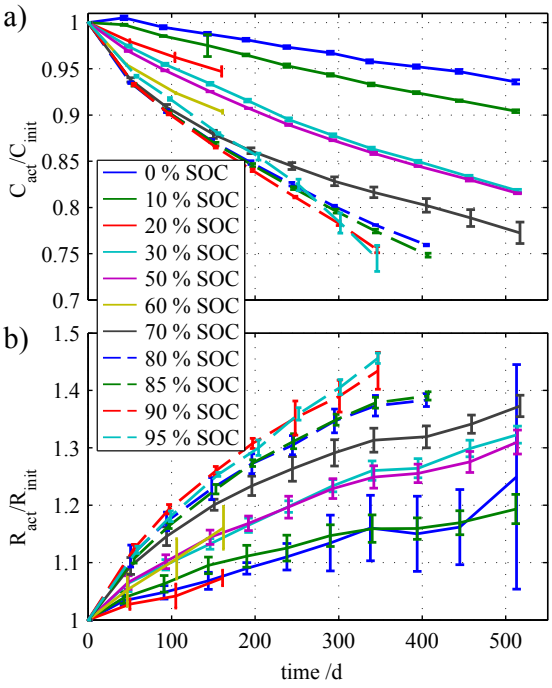

Figure 5: a) Normalized capacity over time and b) normalized resistance over time for calendar aging tests at 50 °C. For each SOC the average on three cells under tests is shown.

For all tests a mean capacity loss and resistance increase has been calculated for every checkup. An error bar plot of both capacity and resistance in the 50 °C tests can be found in figure 5. The cells suffer increasing capacity loss and

resistance increase with higher storage SOC and thereby higher voltage. Also the tests not displayed here with different temperatures show the expected increased aging with higher temperatures.

3.1 Fit method

To obtain a lifetime model out of the accelerated aging tests, a mathematical description of the aging processes is needed. The analysis was split into calendar and cycle aging. In the calendar aging tests, temperature and storage voltage were varied; a function should include these factors.
From figure 5 it can be seen, that different test conditions have unequal checkup numbers. This is due to the removal of cells which went below 75 % of initial capacity or a later start after the first tests were done. For an aging function being directly fitted to all checkups this would have lead to variable impacts of different test conditions on the result. The influence of tests with moderate aging would have been overestimated while new started tests or tests with higher aging and therefore fewer checkups would have been underestimated.
To avoid this a two step fitting was done. In the first step, every single aging condition was fitted using a different fitting function which ideally had only one aging factor. Afterwards the dependency of this aging factor on temperature and voltage was analyzed.

3.2 Time dependency

For a cell with a carbon based anode, like the one used here, it is widely accepted in literature [9, 10] that the dominant calendar aging effect is the formation of a so called solid electrolyte interphase (SEI). The SEI is built up of decomposition products of the electrolyte, consuming lithium during formation and increasing resistance through the growing layer thickness [11]. Although there are different theories on SEI formation [12, 13], both lead to a square root of time dependency. For some already published aging tests [8, 12] this seems to be approved. Nevertheless the capacity decrease measured at this cell started with lower aging and seemed to have a share of linear aging which was also observed in [14]. Therefore a pure linear and a pure square root function are used together with a superposition of both and a function with $t^{0.75}$ as a medium function.

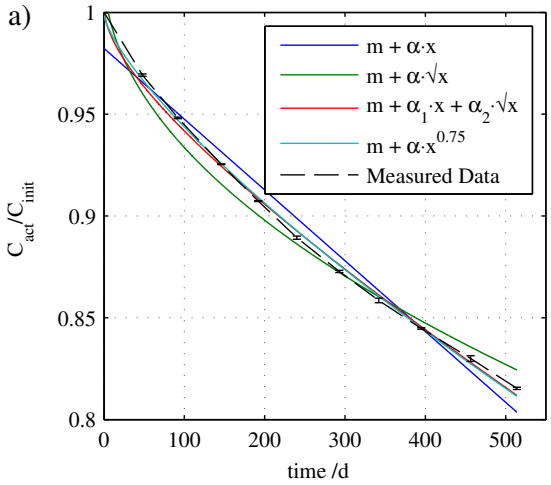

Figure 6: Mean capacity for the cells stored at 50 °C and 50 % SOC over time together with 4 different fit functions.

$$C/R = n \mp \alpha \cdot t \quad (1)$$

$$C/R = n \mp \alpha \cdot \sqrt{t} \quad (2)$$

$$C/R = n \mp \alpha_1 \cdot t \mp \alpha_2 \cdot \sqrt{t} \quad (3)$$

$$C/R = n \mp \alpha \cdot t^{0.75} \quad (4)$$

For all fit functions the parameter n should be equal to 1 as all data is normalized to initial values. Anyway this parameter is set free for the fit to compensate deviations of the measured data. For further analysis only the aging factors α are used.
An example of the fit functions can be found in figure 6. The mean capacity of cells stored at 50 °C and 50 % SOC is plotted together with the fit functions, showing a bad congruence of single linear (1) and square root functions (2). The superposed linear and square root function (3) and the function with $t^{0.75}$ (4) are similar and match the data well. The fit parameters for 50 °C and 50 % can be found in table 1 together with an average R^2 for all tests. Best results on the single tests were obtained using the superposed function (3), but the aging factors α_1 and α_2 do not have a clear trend over voltage.This might be due to scattering of the data which prohibits an exact division into linear and square root functions.

Table 1: Fit parameter for capacity and resistance from the 50 °C and 50 % SOC test. Four different fit functions with three to four free parameters were used. ØR^2 is the mean R^2 value of all fitted tests.

	$n \mp \alpha \cdot t$		$n \mp \alpha \cdot \sqrt{t}$		$n \mp \alpha_1 \cdot t \mp \alpha_2 \cdot \sqrt{t}$		$n \mp \alpha \cdot t^{0.75}$	
	Capacity	Resistance	Capacity	Resistance	Capacity	Resistance	Capacity	Resistance
n	0,982	1,045	1,020	0,981	1,003	0,995	0,999	1,017
α	0,00035	0,00055	0,00862	0,01402			0,00173	0,00278
α_1					0,00018	0,00015		
α_2					0,00427	0,01037		
R^2	0,978	0,949	0,975	0,988	0,997	0,994	0,998	0,986
ØR^2	0,974	0,952	0,960	0,965	0,997	0,987	0,989	0,978

Therefore the function with $t^{0.75}$ is used for further analysis of the aging parameters. This function shows a similar shape in the required range and has only one aging factor which needs to be evaluated. The average R^2 value is not as good as the one from the superposed function, but better than the single linear or square root functions.

3.3 Voltage depedency

A plot of the aging factors over voltage for all tests performed at 50 °C both for resistance and capacity can be found in figure 7. The aging factors show a linear trend considering the whole voltage range. In contrast other papers found an exponential dependency [2] that is clearly not given here. Other work also done on these data sets [15] proposed a correlation between aging and phase changes in the anode material, dividing the voltage dependency in single steps with nearly equal aging.

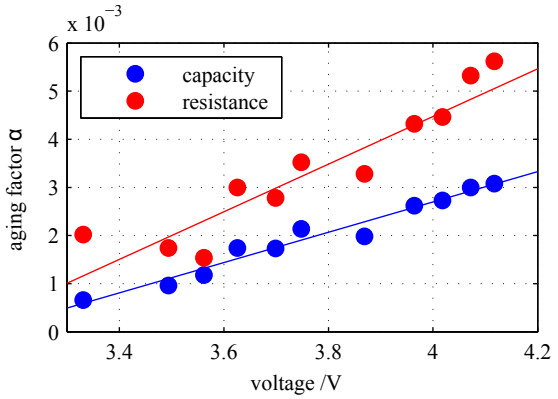

Figure 7: Voltage dependency of the aging factor α over voltage from $C = n - \alpha \cdot t^{0.75}$ for tests performed at 50 °C together with a linear regression.

For an aging model the small differences between a maybe stepwise function and a simple linear dependency can be neglected. For most applications voltage and SOC are changing during the simulated profile, sweeping over areas which underestimate or overestimate the aging. In total these effects should compensate over the full range. Therefore a linear regression was used to describe the voltage dependency. This also has the advantage that only a few data points are used, a stepwise definition would need at least two points per step and increase time and effort significantly.

3.4 Temperature dependency

For temperature dependency only three different temperatures were tested. A lot of literature already described the Arrhenius equation

$$\text{aging factor } \alpha \propto \exp\left(-\frac{E_A}{RT}\right) \qquad (5)$$

as a good matching function for temperature dependency. E_A is thereby the activation energy of a reaction happening at a temperature T, R is the gas constant. To test this equation with our data, a plot of $\ln(\alpha)$ over inverse temperature is shown in figure 8. The three temperatures were 35 °C, 40 °C and 50 °C. For both capacity and resistance the logarithm of aging factors give a linear dependency, confirming the applicability of the Arrhenius equation for these cells. Results of the linear interpolation are activation energies of 58,0 $\frac{\text{kJ}}{\text{mol K}}$ for the capacity and 49,8 $\frac{\text{kJ}}{\text{mol K}}$ for the resistance.

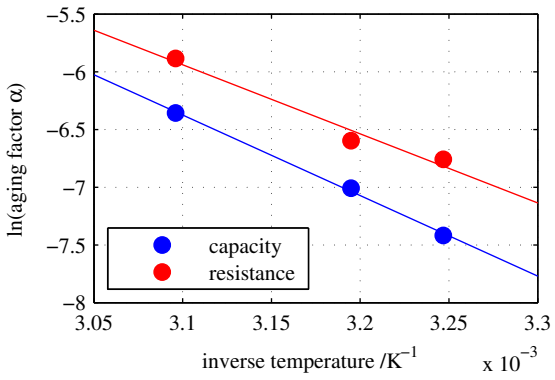

Figure 8: Arrhenius plot of aging factors α for both capacity and resistance over inverse temperature. The shown temperatures are 35 °C, 40 °C and 50 °C. Also the linear regression for temperature dependency is shown.

3.5 Fit function calendar aging

For a mathematical model of calendar aging the dependencies on voltage and temperature need to be combined. Here an aging factor α is used to describe the aging rate during a test of time t.

$$C = 1 - \alpha_{cap} \cdot t^{0.75} \quad (6)$$

$$R = 1 + \alpha_{res} \cdot t^{0.75} \quad (7)$$

The test at 50 °C and 50 % is included both in voltage and temperature fit and therefore chosen as an intersection for both functions. The combined aging factors for capacity and resistance are

$$\alpha_{cap} = (7.543 \cdot V - 23.75) \cdot 10^6 \cdot e^{-\frac{6976}{T}} \quad (8)$$

$$\alpha_{res} = (5.270 \cdot V - 16.32) \cdot 10^5 \cdot e^{-\frac{5986}{T}} \quad (9)$$

for tests done at a voltage V and an absolute temperature T. These equations allow one to calculate the calendar aging for arbitrary conditions of voltage and temperature. They are the basis for the cycle aging analysis in the next chapter.

4 Cycle aging

Cycling a battery leads to additional aging due to processes which do not occur during calendar aging. During intercalation and de-intercalation the material experiences a volume change which is a stress factor for the battery system. Results can be a crack-and-repair of the SEI which consumes lithium and increase the inner resistance or a contact loss of active material particles.
A lot of cycle aging tests varying cycle depth and average SOC were performed. All cycle aging tests were done at a temperature of 35 °C and a current of 1C. This would result in 12 equivalent full cycles per day, but real values are lower due to time for checkups and other unplanned rest periods.
During the time of cycling calendar aging also occurs. To get an analysis of the 'pure' cycle aging, all test data had to be adjusted by the calendar aging. The calendar capacity loss and resistance increase were calculated using the functions obtained from the tests discussed before and then added/subtracted from the measured capacities and resistances. All discussion of cycle aging in this chapter refers to these adjusted values. A selection of typical 'pure' cycle aging curves can be found in figure 9.

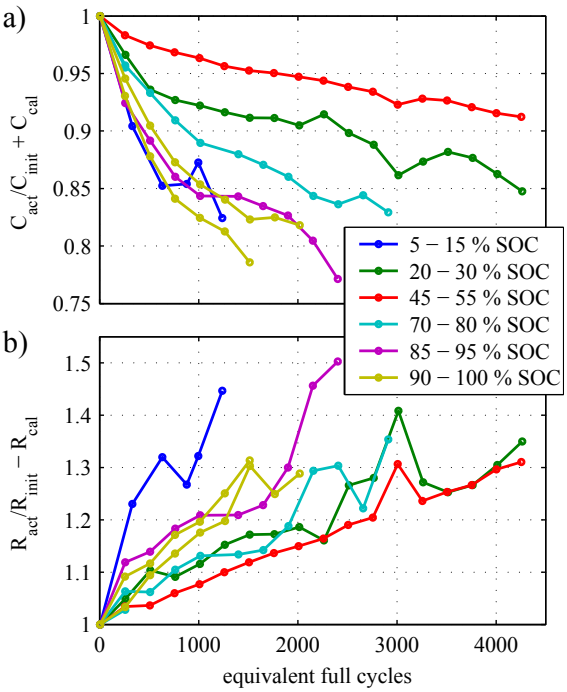

Figure 9: a) Normalized capacity and b) normalized resistance over equivalent full cycles. Values are adjusted to the 'pure' cycle aging by subtracting the calculated calendar aging. The shown tests were done with 1C at 35 °C and a cycle depth of 10 %.

Within literature sometimes a linear aging over charge throughput Q is found [16], but also work about square root aging was presented [7, 17].

In our tests we found two different dependencies for capacity and resistance. For capacity loss a clear square root function can be found while the resistance increase is linear. This indicates that during cycling two different aging processes occur in the battery, one that has a strong impact on capacity and another that influences resistance.

$$C_{cyc} = 1 - \beta_{cap} \cdot \sqrt{Q} \quad (10)$$

$$R_{cyc} = 1 + \beta_{res} \cdot Q \quad (11)$$

Analysis was done with a two step fitting like before. In the first step, all single tests were fitted using equation (10) and (11).

4.1 Dependency on cycle depth

Cycle depth is an important point to battery aging. For a lot of battery types and chemistries, deep cycles cause disproportional or exponential stronger aging compared to small cycle depths [18]. In these cases oversizing of battery capacity is a effective but also expensive option. With a good knowledge of cycle depth dependency, the oversizing can be reduced to a minimum.
The used cells show a non-exponential dependency, instead a more linear trend can be found. For capacity loss this linear dependency seems to be true for the full range while the resistance increase shows a constant minimal aging for low cycle depths.

4.2 Dependency on average voltage

Figure 9 already indicates that cycling around a middle voltage leads to the lowest aging. Both for capacity loss as well as for resistance increase, the cycling between 45 and 55 % SOC has the smallest effects. Cycling around lower or higher voltages increases the cycle aging rate.
For all cycle depth a U-shaped function can be found with a minimum around 3.7 V average voltage. The dependency on average voltage is much higher for capacity loss than for resistance increase.
For lifetime optimized charging strategies the dependency on average voltage has to be taken into account. From calendar aging aspects the lower SOC has advantages, but with cycling the optimum might shift to an average SOC level.

4.3 Total fit function

With the aforementioned linear cycle depth (ΔDOD) and quadratic average voltage ($\O V$) dependency a fit was made to all aging factors β from the cycle aging tests. The resulting functions for cycling capacity loss and resistance increase are

$$\beta_{cap} = 8.175 \cdot 10^{-3} \cdot (\O V - 3.683)^2 \ldots + 7.057 \cdot 10^{-4} + 4.198 \cdot 10^{-5} \cdot \Delta\text{DOD} \quad (12)$$

and

$$\beta_{res} = 2.673 \cdot 10^{-4} \cdot (\O V - 3.741)^2 \ldots - 1.900 \cdot 10^{-5} + 2.837 \cdot 10^{-6} \cdot \Delta\text{DOD}. \quad (13)$$

The total aging function is then the superposition of calendar and cycle aging as shown in equation (14) and (15). With this function a calculation of battery aging and lifetime is possible for all conditions.

$$C = 1 - \alpha_{cap} \cdot t^{0.75} - \beta_{cap} \cdot \sqrt{Q} \quad (14)$$

$$R = 1 + \alpha_{res} \cdot t^{0.75} + \beta_{res} \cdot Q \quad (15)$$

5 Model

To calculate lifetime and battery aging, the voltage and temperature of the battery are needed. Most applications only provide a current or power profile. Therefore a holistic model was built which consists of three parts:

- Impedance based electric model
- Thermal model
- Aging model.

These three model parts are called in a loop. A schematic of this integrated model is shown in figure 10. As the model is impedance based it does a fast computation and can easily be parameterized through electrochemical impedance spectroscopy (EIS) measurements.
The aging model is based on the equations developed from the accelerated aging tests. Every aging parameter was analyzed separately and put into a mathematical equation, therefore the effects can be extrapolated to ranges that have not been tested (e.g. lower temperatures).

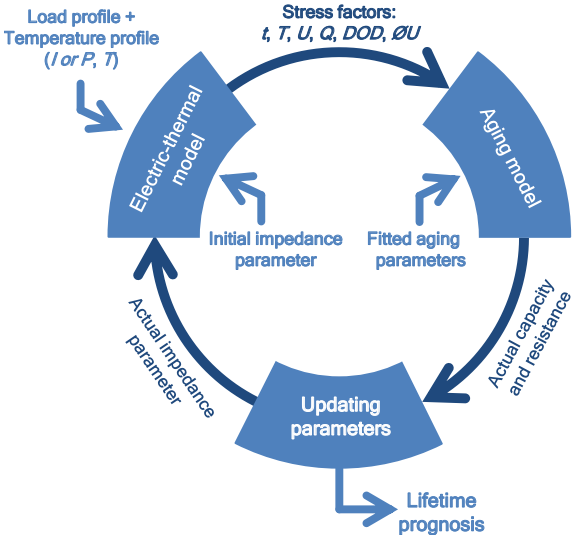

Figure 10: Graphical representation of the holistic model. Calculation is done in a loop with load profile, impedance parameters and aging factors as input. Output is the remaining capacity and resistance together with a lifetime estimation.

The model takes a load profile (can be power or current) as input. Furthermore a profile for ambient air temperature can be included, else a constant temperature is chosen.

The impedance based electrical model uses an equivalent electric network that consists of a series resistance, two ZARC elements and an OCV source.

A thermal model is coupled to the electric model. Heat production is based on ohmic losses calculated by the electric model. Heat transfer to the ambient air is modeled as heat conductivity with variable factor to match different mounting scenarios.

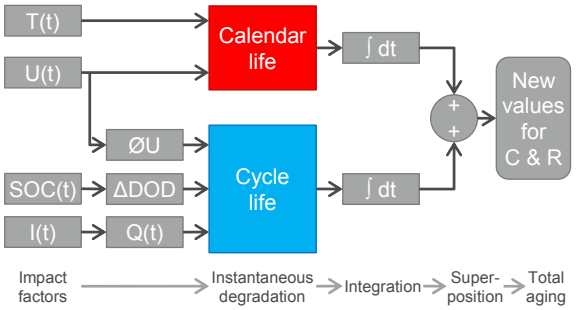

Figure 11: Schematic of the calculation process within the aging model. Input values are given for every single time step, calendar and cycle life aging are integrated on these single aging steps.

Voltage, temperature, SOC and current are taken from the combined electric-thermal model as inputs for the aging model. From this data cycle depth and average SOC are calculated. The average voltage for cycle aging is only calculated during current flow, rest periods do not influence it. Calendar and cycle life aging is calculated for every single time step using the aging functions gained from the accelerated aging tests. Calendar and cycle aging are added to get the total aging. A schematic of the aging calculation is given in figure 11.

6 Verification

Along with the accelerated aging tests a verification profile has been applied to the batteries. For this verification profile a driving cycle was used together with charge and rest periods. The driving profile was taken from real car measurements done in Aachen, including city and highway driving. The power was scaled down to meet the specification of the battery.
Three different test profiles were built with this load profile. Plots are displayed in figure 12. The first and second profile consist of two driving

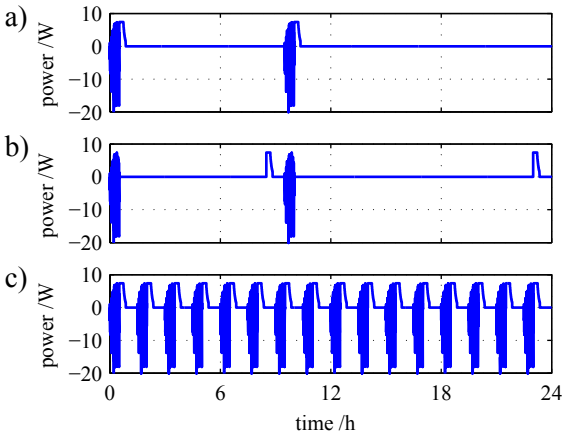

Figure 12: Three power profiles over time for model evaluation. a) Charge after driving, b) charge before driving and c) no rest periods.

parts a day separated with long rest periods. The first profile has the charge periods just after the driving part while the second one charges before driving. The third profile is an alternation of driving and charging without long rest periods. The charging in all three profiles is performed with 1C.

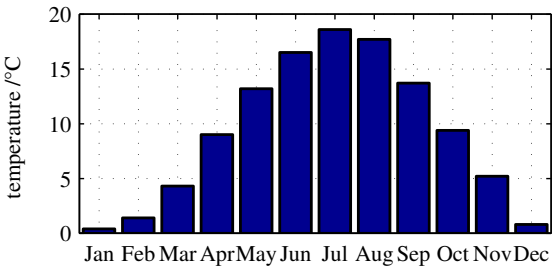

Figure 13: Temperatures used for model verification. For each month an ambient temperature is given to the simulation. Values are average temperatures for Germany from 2001 - 2010.

The profiles tests were performed with monthly changing ambient air temperature. The temperatures are average values for Germany from 2001 to 2010 [19]. A diagram of the temperatures is shown in figure 13. The initial month for the verification was September. Temperatures inside a battery pack build in a car might be higher than the ambient air temperature. Therefore higher temperatures have also been tested. Tests with all three profiles have also been performed at the average temperatures plus 10 °C and at plus 20 °C.

Checkups on these cells have been done every month with the same method like the other cycle life tests described in chapter 2.3.

The measured data for both capacity loss and resistance increase for the verification profiles can be found in figure 14 together with the simulation results. The figure shows that the aging predicted by the model matches the measurements well for capacity loss although the model was only parameterized at temperatures much higher than the temperatures applied in the verification profile. The extrapolation using the Arrhenius equation (5) seems to be valid down to temperatures at 0 °C.

The simulated resistances for most verification profiles are lower than the measured ones. The biggest relative deviation is found in cases where the simulated resistance increase is very small, for higher aging rates measurement and simulation match better.

As this cell shows only a small resistance increase in comparison with the capacity loss, the last one will limit the lifetime for nearly all application. Therefore the correct capacity prediction is more valuable than the resistance simulation.

7 Conclusion

In this work an aging model for an 18650 cell with NMC cathode chemistry was established. An extensive set of both calendar and cycle aging tests has been performed including more than 60 cells. Varied parameters were voltage/SOC and temperature for the calendar tests. In the cycle aging tests cycle depths and average voltage were studied. During all tests checkups with actual capacity and inner resistance were determined.

Using these values for capacity fade and resistance increase mathematical functions were fitted. For both calendar and cycle aging tests a two step fitting was done. The resulting fitting functions include the dependency of capacity and resistance on time respectively charge throughput and the other varied parameters.

For the tested cell the calendar aging could not be modeled using a square root function of time. The data indicated the occurrence of a second main aging effect besides normal SEI growth which has a linear time dependency. As both effects could not be separated by the fit a $t^{0.75}$ dependency was used. For temperature dependency the Arrhenius equation was used. On this cell the aging speed increased linearly with voltage for a calendar aging test.

The cycle aging data was adjusted by the calendar aging prediction. Fits were done with two different functions for capacity loss and resistance increase. The capacity was implemented using a square root function of charge throughput while the resistance had a linear dependency. Both capacity and resistance had the lowest aging while cycling around 3.7 V (50 % SOC), lower or higher cycle ranges increased aging. The effect of cycle depth on aging was linear.

The fit functions were implemented in an aging model which was coupled to an impedance based electric-thermal model. Three different verification profiles were also tested on the cells, each at three temperature levels. In all nine cases the predicted capacity loss matched the measured data. For low resistance increase the model underestimated the aging, for higher resistance increase the congruence is quite good.

This holistic model is able to predict the aging for different drive cycles and management strategies. It can be used with current and power pro-

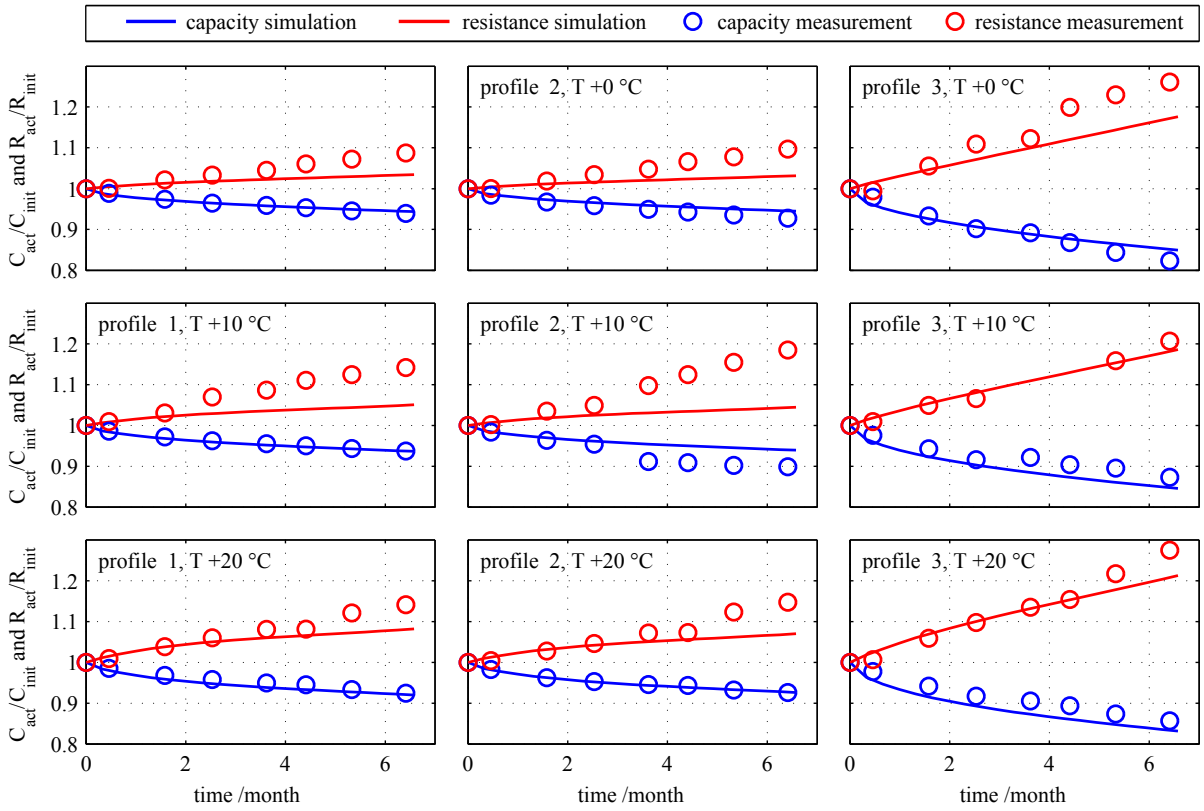

Figure 14: Comparison between measured data (circles) and simulation results (lines). Three profiles were tested at three temperature levels. Both capacity and resistance are shown for each test.

files as input, also ambient air temperature profiles changing over the seasons can be included. The model is a powerful tool to optimize BMS strategies and lifetime for all applications using this cell.

8 Acknowledgment

The project upon which this publication is based was funded by the Federal Ministry of Education and Research under project numbers 16N12035 (eProduction) and 13N10656 (e performance) as well as by the Impuls- und Vernetzungsfond der Helmholtz-Gemeinschaft e.V. through the framework of the research initiative HGF Energie Allianz. The authors of this publication are responsible for its content.

References

[1] S. Käbitz et al. *Cycle and calendar life study of a graphite|$LiNi_{1/3}Mn_{1/3}Co_{1/3}O_2$ Li-ion high energy system. Part A: Full cell characterization*. J. Power Sources. ISSN 0378-7753, 239(2013), 572 – 583.

[2] M. Ecker et al. *Development of a lifetime prediction model for lithium-ion batteries based on extended accelerated aging test data*. J. Power Sources. ISSN 0378-7753, 215(2012), 248 – 257.

[3] E. Thomas et al. *Statistical methodology for predicting the life of lithium-ion cells via accelerated degradation testing*. J. Power Sources. ISSN 0378-7753, 184(2008), 312 – 317.

[4] E. Thomas et al. *Rate-based degradation modeling of lithium-ion cells*. J. Power Sources. ISSN 0378-7753, 206(2012), 378 – 382.

[5] B. Y. Liaw et al. *Modeling capacity fade in lithium-ion cells*. J. Power Sources. ISSN 0378-7753, 140(2005), 157 – 161.

[6] M. Safari et al. *Multimodal Physics-Based Aging Model for Life Prediction of Li-Ion Batteries*. J. Electrochem. Soc., 156(2009), A145–A153.

[7] J. Wang et al. *Cycle-life model for graphite-$LiFePO_4$ cells*. J. Power Sources. ISSN 0378-7753, 196(2011), 3942 – 3948.

[8] I. Bloom et al. *Mechanisms of impedance rise in high-power, lithium-ion cells*. J. Power Sources. ISSN 0378-7753, 111(2002), 152 – 159.

[9] M. Broussely et al. *Main aging mechanisms in li ion batteries*. J. Power Sources. ISSN 0378-7753, 146(2005), 90 – 96.

[10] J. Vetter et al. *Ageing mechanisms in lithium-ion batteries*. J. Power Sources. ISSN 0378-7753, 147(2005), 269 – 281.

[11] E. Peled. *The Electrochemical Behavior of Alkali and Alkaline Earth Metals in Non-aqueous Battery Systems - The Solid Electrolyte Interphase Model*. J. Electrochem. Soc., 126(1979), 2047–2051.

[12] M. Broussely et al. *Aging mechanism in Li ion cells and calendar life predictions*. J. Power Sources. ISSN 0378-7753, 97 - 98(2001), 13 – 21.

[13] H. J. Ploehn, P. Ramadass and R. E. White. *Solvent Diffusion Model for Aging of Lithium-Ion Battery Cells*. J. Electrochem. Soc., 151(2004), A456–A462.

[14] J. Belt, V. Utgikar and I. Bloom. *Calendar and PHEV cycle life aging of high-energy, lithium-ion cells containing blended spinel and layered-oxide cathodes*. J. Power Sources. ISSN 0378-7753, 196(2011), 10213 – 10221.

[15] M. Ecker et al. *Calendar and cycle life study of NMC-based 18650 automotive lithium-ion batteries*. J. Power Sources, submitted for publication.

[16] K. Takei et al. *Cycle life estimation of lithium secondary battery by extrapolation method and accelerated aging test*. J. Power Sources. ISSN 0378-7753, 97 - 98(2001), 697 – 701.

[17] R. Wright et al. *Power fade and capacity fade resulting from cycle-life testing of advanced technology development program lithium-ion batteries*. J. Power Sources. ISSN 0378-7753, 119 - 121(2003), 865 – 869.

[18] D. U. Sauer. *SECONDARY BATTERIES - LEAD-ACID SYSTEMS | Lifetime Determining Processes*. In J. Garche, editor, *Encyclopedia of Electrochemical Power Sources*. Elsevier, Amsterdam (2009). ISBN 978-0-444-52745-5, pages 805 – 815.

[19] Deutscher Wetterdienst. *Zeitreihen von Gebietsmitteln*. `http://www.dwd.de/bvbw/appmanager/bvbw/dwdwwwDesktop?_nfpb=true&gsbSearchDocId=809418` (2013).

Authors

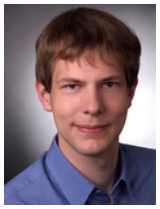

Johannes Schmalstieg received his diploma in Physics from TU Dortmund University in 2011. In November 2011 he joined ISEA as research associate. His areas of interest are semi-empirical aging models for lithium-ion batteries.

Stefan Käbitz received his diploma degree from the RWTH Aachen University in 2010. In March 2010 he joined ISEA as research associate. Since April 2011 he is team leader for ISEAs activities in the field of lithium-ion batteries. His areas of interest are impedance-based as well as physico-chemical models for lithium-ion batteries with a special focus on EIS.

Madeleine Ecker received her diploma in Physics from University of Heidelberg in 2009. In July 2009 she joined ISEA as a research associate. From October 2010 till September 2012 she was team leader for ISEAs activities in the field of modeling. Now she is deputy Head of the section Modeling, Analytics and Lifetime Prediction. Her areas of interest are empirical as well as physico-chemical modeling of lithium-ion batteries with a special focus on cell aging.

Dirk Uwe Sauer received his diploma in Physics from University of Darmstadt in 1994. From 1994 to 2003 he worked at Fraunhofer ISE as a research scientist, from 2000 2003 as team leader for Storage Systems. After receiving his PhD from University of Ulm in 2003, topic: ”Optimisation the usage of lead-acid batteries in photovoltaic-hybrid systems with special emphasis on battery aging”, he joined ISEA as professor for Electrochemical Energy Conversion and Storage Systems.